Sensors and Actuators B 238 (2017) 962–971

Contents lists available at ScienceDirect

Sensors and Actuators B: Chemical

journal homepage: www.elsevier.com/locate/snb

Electrochemical bisphenol A sensor based on exfoliated Ni_2Al-layered double hydroxide nanosheets modified electrode

Tianrong Zhan[a,*], Yang Song[a], Zhengwei Tan[a], Wanguo Hou[b,*]

[a] Key Laboratory of Sensor Analysis of Tumor Marker (Ministry of Education), State Key Laboratory Base of Eco-Chemical Engineering, Qingdao University of Science and Technology, Qingdao 266042, China
[b] Key Laboratory of Colloid & Interface Chemistry (Ministry of Education), Shandong University, Jinan 250100, China

ARTICLE INFO

Article history:
Received 29 April 2016
Received in revised form 23 July 2016
Accepted 26 July 2016
Available online 27 July 2016

Keywords:
Exfoliated layered double hydroxide nanosheets
Bisphenol A
Differential pulse voltammetry
Electrochemical oxidation

ABSTRACT

In the present work, the ultrathin exfoliated Ni_2Al layered double hydroxide (ELDH) nanosheets were prepared by using L-asparagine as pre-intercalator in aqueous medium. The transmission electron microscopy and atomic force microscopy images displayed that ELDH nanosheets had lost the original hexagon of hydrotalcite with about 200 nm lateral size and less than 3 nm thickness. Then a sensitive electrochemical sensor was fabricated for bisphenol A (BPA) detection based on ELDH modified glassy carbon electrode with aid of film-forming agent chitosan. The proposed sensor showed an efficient electrocatalytic performance on the oxidation of BPA with the enhanced oxidation response and the lowered oxidation overpotential (0.489 V). Differential pulse voltammetry (DPV) was employed for the determination of BPA with a wide linear range from 0.02 to 1.51 μM. The detection limit was calculated as 6.8 nM (S/N = 3). The resultant sensor exhibited good reproducibility, selectivity and acceptable stability due to the contribution of the more active sites and the large surface area from ELDH nanosheets. Additionally, the concentrations of BPA in milk samples were analyzed by this developed method with an acceptable result.

1. Introduction

Bisphenol A (BPA, 2,2-bis(4-hydroxyphenyl)propane), the important monomer and plasticizer, has a high production volume more than six billion pounds produced worldwide each year [1]. BPA can be used as the raw materials for the synthesis of polyester resins, epoxy resins, polycarbonate plastics, flame retardants, and other special products, which are extensively used in wide range including food containers or packaging, inner coating of food cans, beverage cans, water bottles, baby bottles, dental sealants and drug delivery systems [2]. Owing to the generous use of BPA-based products in daily living, BPA is present in a wide array of food, water, air, soil and the bodies of living organism and human [3]. Unfortunately, BPA can interfere with hormonal activities in the growth, thereby giving rise to the sexual dysfunction or differentiation, the impaired immune function and the enhanced cancer risk of various cancers (e.g. testicular, prostate and breast cancer) even at very low concentration [4,5]. For the sake of public health and safety, development of a highly sensitive, selective, and reliable method for BPA detection is a fairly important task.

The techniques based on chromatography coupling with fluorescence, ultraviolet or mass spectrometry are high sensitive methods for the determination of BPA. However, the disadvantages of expensive instrument, cumbersome sample pretreatments and professional operators greatly reduce their applicability [6]. Enzyme linked immunosorbent assay [7], molecular imprinting [8] chemiluminescence [9], surface-enhanced Raman scattering [10] and fluorescence techniques [11] have also been developed for the detection of BPA. By comparison, electrochemical sensors have widely employed as an acceptable technique because of their reliability, instrument simplicity, simple operation, timesaving, excellent sensitivity, fast and real-time in situ analysis [12,13]. Although an electro-active species containing phenolic structure, detecting BPA on bare electrode is inapplicable because of the irreversible fouling. Additionally, the involving high overpotential can increase the interference of analysis and result in low selectivity and sensitivity [14,15].

It is well known that sensing materials are crucial to the performance of electrochemical sensor. As a result, different nanoparticlels have been used as modifiers to advance the electrochemical signals of BPA. For example, carbon support materials

* Corresponding authors.
E-mail addresses: trzhan@sdu.edu.cn (T. Zhan), wghou@sdu.edu.cn (W. Hou).

http://dx.doi.org/10.1016/j.snb.2016.07.151
0925-4005/

(carbon nanotube, graphene, porous carbon and carbon nanowires) [16], mesoporous silica [17], quantum dots [18], ferroferric oxides [8], aptamer-gold [19] and tyrosinase-rGO [5] have been successfully employed as interface matrices for BPA monitoring. Layered double hydroxide (LDH), also named as hydrotalcite-like or anionic clays, presents a class of lamellar solid with the chemical composition formula of $[M_{1-x}^{II}M_x^{III}(OH)_2]^{x+}[(A^{n-})_{x/n}\cdot mH_2O]$, where M^{II} and M^{III} respectively stand for divalent and trivalent metal cations in the hydrotalcite layers. The isomorphous substitution of M^{II} by M^{III} brings out the positively charged hydrotalcite-like layers balanced by the interlayer anions (A^{n-}) and water molecules. In LDH nanostructure, the octahedral MO_6 blocks share their edges to form the extended 2D sheets, in which metal cations and hydroxide anions are respectively located in the centers and the vertexes of octahedra. Recently, LDH has shown the promising application prospect in electro-catalysis, adsorption, drug deliver and biotechnology owing to their desirable ion-exchange capability, open layered structure, positive charge nature, high surface area and better biocompatibility [20–23]. Specifically, several classes of LDH have been used as sensing materials for fabrication of phenol sensors or biosensors. Shan et al. have fabricated phenol biosensors by immobilizing polyphenol oxidase on LDH modified electrode [24]. An amperometric phenol biosensor has been developed using chitosan/LDH hybrid as modifier [25]. Yin et al. have constructed the BPA electrochemical sensor by LDH modified electrode [15]. Our group has also designed an ionic functionalized LDH modified electrode for BPA sensitive determination [26]. Although the better electrocatalytic potential of LDH to BPA, the strong tendency to form agglomerates only affords the low electron transportation and the preservation of most MO_6 active sites in LDH aggregates has not yet exerted their perfect catalytic performance. The exfoliation is an effective solution to obtain well dispersed LDH nanoplatelets with more MO_6 active sites exposed and accessible. As a result, exfoliated LDH nanosheets can offer an enhanced elelctrochemical surface area and a decreased mass transfer resistance, thereby guaranteeing the efficient entrapment and the high electrocatalytic activity toward substrate [21]. However, the single- or several-layer LDH nanosheets have been not yet used to fabricate an electrochemical sensor for electrocatalysis investigation of BPA.

Recent years, exfoliation of LDH in amino acids aqueous solution has emerged as an efficient approach to produce two-dimensional LDH nanosheets with high surface activity relative to their bulk counterparts [27]. In the present work, therefore, the water soluble amino acid of L-asparagine [$H_2NCOCH_2CH(NH_2)COOH$], with similar structure to formamide, was employed as pre-intercalator for LDH delamination in aqueous medium. We assumed that exfoliation of LDH could not only improve the accessibility to inner surface of host matrixes, but also enhance the electrocatalytic activity of anisotropic hydrotalcite-like nanosheets. Therefore, only the 2D positively charged LDH nanosheets without any conductive component were further used to prepare the modified electrode for study of the behaviors and determination of BPA. The electrochemical performance of LDH nanosheets was also compared with the bulk LDH counterpart, which might demonstrate the establishment of a BPA sensor with desirable properties.

2. Experimental

2.1. Reagents and apparatus

BPA and chitosan were respectively purchased from Aladdin Chemistry Co. (Shanghai, China) and Beijing Chemical Co., (China). Other chemicals were directly used as analytical grade without further purification.

Electrochemical measurements were performed on CHI660D electrochemical workstation (CHI, China). A three-compartment electrochemical cell contained a modified glassy carbon electrode (GCE, Φ = 3 mm) as working electrode, a platinum wire and a saturated calomel electrode (SCE) respectively as auxiliary electrode and reference electrode. X-ray power diffraction (XRD) patterns were collected using a Rigaku DLMAX 2550 V diffractometer (Japan) with Cu Kα radiation (λ = 0.154178 nm, graphite monochromator, 28 kV and 20 mA) from 3° to 70° with a scanning speed of 10° min^{-1}. Morphology of solid sample was evaluated by a JSM-2000EX transmission electron microscope (TEM, Japan) and a JSM-6610 scanning electron microscope (SEM, Japan). Atomic force microscopy (AFM) images were recorded using a Seiko SPA 400 controller by DFM/Tapping model.

2.2. Synthesis and exfoliation of LDH

2.2.1. Synthesis of Ni2Al-NO3− LDH

According to the our previous report [26], $NiCl_2{\cdot}6H_2O$, $AlCl_3{\cdot}6H_2O$, and urea were uniformly dissolved in 1000 mL of deionized water with their final concentrations as 10, 5, and 35 mM, respectively. Then, under magnetic stirring, the mixed solution was heated for 48 h at 97 °C. The green Ni_2Al-LDH solid was collected as CO_3^{2-} type (LDH-CO_3^{2-}) by centrifugation and washed with deionized water and anhydrous ethanol. Then 1.0 g of LDH-CO_3^{2-} was dispersed into 1000 mL of mixed aqueous solution of 1 M NaCl and 3.3 mM HCl. After agitating nitrogen gas for 30 min, the sealed vessel was shaken for 12 h at ambient temperature. The obtained LDH-Cl^- was added to 1000 mL of 0.1 M $NaNO_3$ aqueous solution. After same process as above, LDH-NO_3^- phase was successfully synthesized.

2.2.2. Exfoliation of LDH-NO_3

Enough L-asparagine was added to 300 mL deionized water and stirred for 20 min at 45 °C to form a saturated aqueous solution. Then 0.3 g LDH-NO_3^- was added to the L-asparagine solution. After sonication and purging with nitrogen gas for 15 min, the reactor was sealed and agitated vigorously for 2 days with a speed of 200 rpm at the same temperature. The resulting dispersion was centrifuged for 10 min at 2000 rpm to remove the unexfoliated particles. The upper mixture was stored at 4 °C overnight and then the crystallized L-asparagine was separated by filtration. The exfoliated Ni_2Al-LDH nanosheets (ELDH) were obtained as a light green and translucent colloidal suspension. The above suspension was concentrated to ELDH concentration as 3 mg/mL.

2.3. Preparation of ELDH/GCE

The GCE was polished to a mirror-like surface with 0.05 μm alumina powder and thoroughly cleaned with redistilled water before modification. Then, 8 μL ELDH suspension was cast on the clean GCE surface with a microinjector. Afterward, 3 μL of 0.5% chitosan acetic acid solution was coated on the ELDH modified electrode and dried at room temperature. The resultant modified electrode was denoted as ELDH/GCE. For comparison, LDH-CO_3^{2-} modified GCE (LDH/GCE) was fabricated by the similar procedure. The procedure for the materials preparation and electrochemical sensor fabrication are illustrated in Scheme 1.

2.4. Preparation of real sample for determination

The fresh liquid milk and milk powder were purchased from Liqun supermarket (Qingdao, China). According to the literature [28], 5.0 mL of liquid milk was first mixed with 25 mL PBS solution. After one hour sonication, the mixture was centrifuged at 12000 rpm for 15 min. The collected supernatant was diluted with

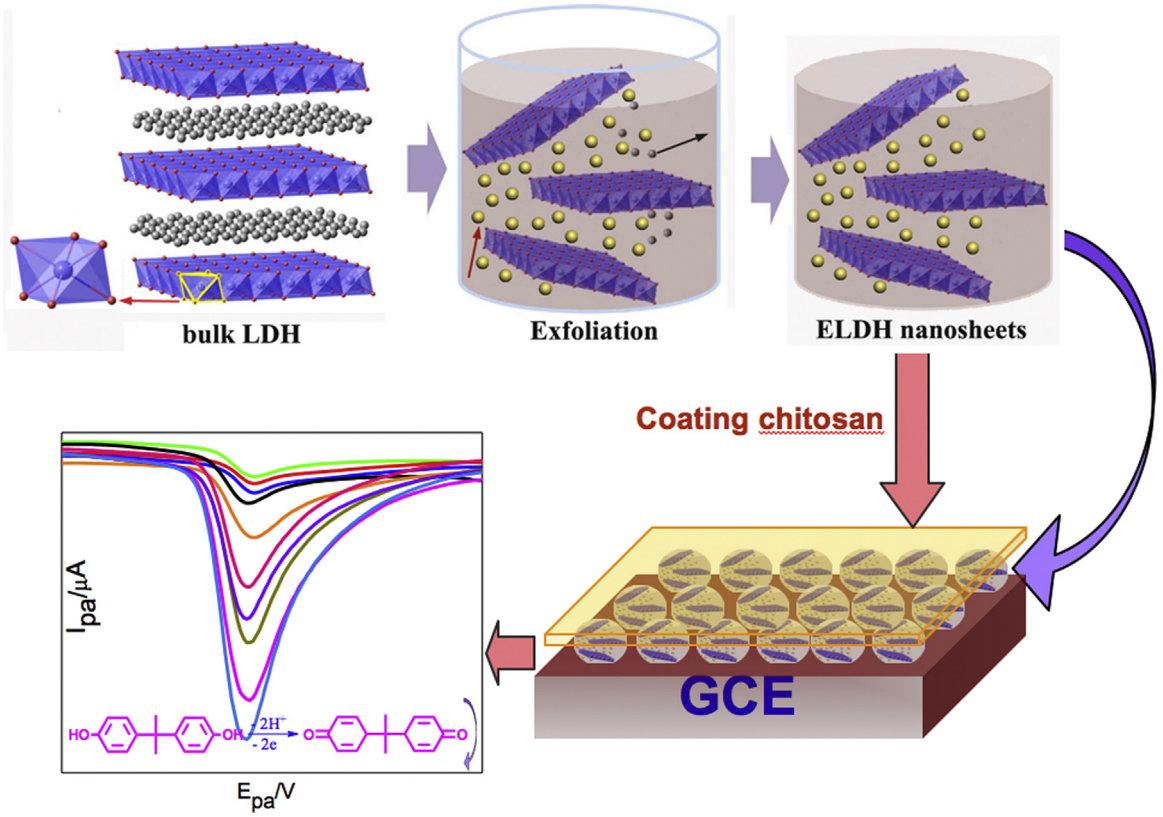

Scheme 1. Schematic representation of materials preparation and electrochemical sensor development.

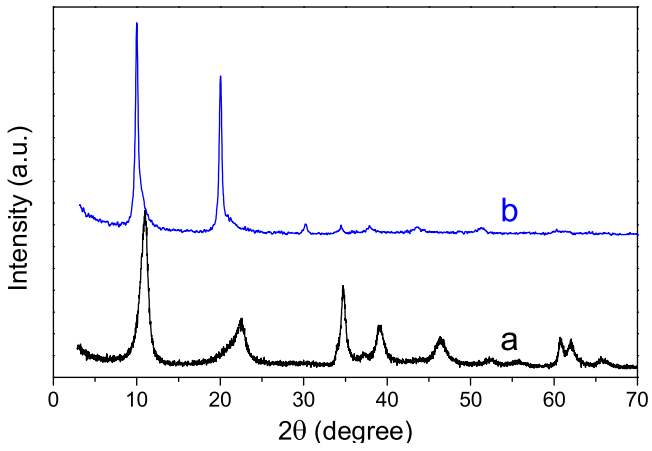

Fig 1. XRD patterns (B) of LDH-CO_3^{2-} (a) and LDH-NO_3^- (b).

PBS (pH = 8.5) solution to the calibration line of 25 mL volumetric flask. Finally, the obtained liquid milk sample was used to carry out the BPA standard spiked experiment. The milk powder sample was obtained by the similar procedure as above except that 2.5 g of milk power was used. The samples without containing BPA were used as negative control.

3. Results and discussion

3.1. Structure and morphology characterization of LDH and ELDH

Fig. 1 shows the XRD patterns of LDH-CO_3^{2-} and LDH-NO_3^-. Pristine LDH-CO_3^{2-} (Fig. 1a) presents the sharply characteristic (003), (006), (112), (015), (018), (110), and (113) peaks. Its d_{003} value of 0.758 nm is identical to the previous report for LDH-CO_3^{2-} [26]. The cell parameters of a ($2d_{110}$) and c [$3/2(d_{003} + 2d_{006})$] were respectively calculated as ca. 0.3042 and ca. 2.3486 nm, indexing a hexagonal lattice of LDH with high crystallinity and fine purity [27]. For ELDH preparation, CO_3^{2-} must be removed from the interlayer of LDH. So LDH-NO_3^- phase was firstly synthesized after continuous ion-exchange with Cl^- and NO_3^-. XRD of LDH-NO_3^- (Fig. 1b) displays the shift of typical reflections to lower 2θ with relatively weaker intensity. The d_{003} basal spacing is enlarged to 0.882 nm [29]. These results suggested that LDH-CO_3^{2-} had been completely transferred into LDH-NO_3^- form. The widened interlamellar spacing is preferable for the further exfoliation of LDH.

The pristine LDH-CO_3^{2-} was first prepared by the general solvothermal coprecipitation technique in presence of urea. The obtained crystals are a light green fine powder and can be well dispersed in water. Its TEM image (Fig. 2a) shows the classic hexagonal flakes with the lateral size of 1–2 μm. The slow urea hydrolysis process offers the perfect hydrotalcite morphology with high crystallinity, which is significantly beneficial to the next delamination. After NaCl–HCl treatment and anion exchange by $NaNO_3$, the strongly associated CO_3^{2-} anions were fully replaced by NO_3^- counterparts. Then LDH-NO_3^- were exfoliated in L-asparagine saturated aqueous solution [27]. The as-prepared ELDH colloid solution exhibited a Tyndall effect. The ELDH nanosheets with about 200 nm lateral sizes could be observed from its TEM image (Fig. 2b). After exfoliation, The ELDH particles lost their original hexagon accompanying the emergence of irregular nano-platelets morphology. Some nanosheets were very transparent so that several platelets could be seen through each other. These results revealed that ELDH had ultrathin property and were broken into small sized nanoflakes due to the delamination treatment [29]. The ultrathin nature of ELDH was also confirmed by their AFM result. The image of a 0.8 × 1.2 μm^2 area (Fig. 2c) exhibits that ELDH nanoparticles are not uniformly dispersed and some hydrotalcite

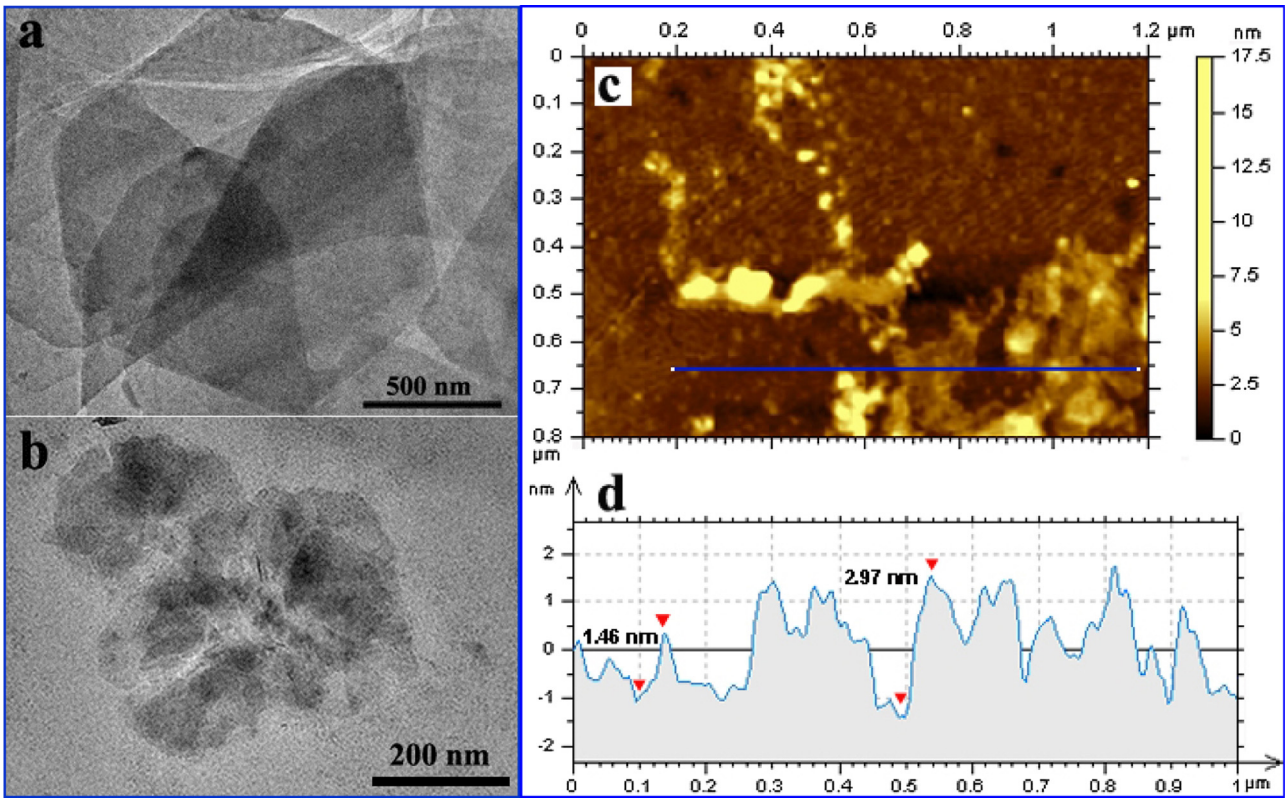

Fig. 2. TEM images of LDH-CO_3^{2-} (a) and ELDH (b); AFM images of a 0.8 × 1.2 μm^2 area of ELDH (c) and cross-sectional analysis along the blue line in c (d). (For interpretation of the references to colour in this figure legend, the reader is referred to the web version of this article.)

flakes are overlapped together. The topographic height was gotten less than 3 nm according to cross-sectional analysis (Fig. 2d). Therefore, single- or multi-layer LDH nanosheets had been successfully prepared, which could make a contribution to enhance the electrocatalytic ability because of large surface area and more active sites exposure.

3.2. Electrochemical characterization of ELDH modified GCE (ELDH/GCE)

To evaluate the electron transfer nature of sensing materials, cyclic voltammograms (CVs) measurements of GCE, LDH/GCE and ELDH/GCE were carried out in 5 mM $Fe(CN)_6^{3-/4-}$ (Fig. 3A). Compared with bare GCE (curve *a*), redox currents of LDH/GCE (curve *b*) are distinctly increased with a smaller peak-to-peak separation (ΔEp) of 96 mV. The results could be ascribed to the fast mass transfer and larger surface-to-volume ratio of LDH nanostructure. While LDH were exfoliated into single- or several layers, the bigger redox peaks were appeared on ELDH/GCE (curve *c*) with the smallest ΔEp value of 81 mV. An apparent increase of electrochemical response demonstrated that the enlarged surface area and much more exposed active sites resulted in the easier electron transfer from bulk LDH to ultrathin ELDH nanosheets. Moreover, the improved electrostatic attraction between the positively charged ELDH and the negatively charged $Fe(CN)_6^{3-/4-}$ probe could also play an important effect on the electrochemical signals. Electrochemical impedance spectroscopy (EIS) was also used to characterize the modified electrode. The linear section of EIS represents the diffusion-limited process, and the semicircle portion relates to the electron transfer-limited process [15,26]. Fig. 3B shows Nyquist diagrams of 5 mM $[Fe(CN)_6]^{3-/4-}$ in 0.1 M KCl at different electrodes. The impedance spectra of three modified electrodes were fitted with the Randles' equivalent circuit (Inset of Fig. 3B), which were well matched with the experimental data. Bare GCE (curve *a*) presents a small well defined semicircle at higher frequencies, suggesting a low transfer resistance. When LDH and ELDH are anchored on GCE surface by film-forming agent chitosan, the impedances of the modified electrodes are dramatically increased because of the non-conductivity of chitosan and LDH in the film. However, by comparison with bulk LDH, ELDH could obviously accelerate the electron stransfer of $Fe(CN)_6^{3-/4-}$. It could be suggested that the more positive charges and exposed active sites of ELDH could attract more $Fe(CN)_6^{3-/4-}$ to the underlying electrode surface.

3.3. Electrochemical behaviors of BPA

Fig. 4 shows CVs of GCE (a), LDH/GCE (b) and ELDH/GCE (c) of 0.1 mM BPA in 0.1 M pH = 8.5 PBS. Only the well-defined oxidation peaks without reduction currents were observed at all the electrodes in selected potential window, indicating a typical of absolutely irreversible electrode reaction [17,30]. Furthermore, the oxidation signals of BPA had completely vanished at third segment during the successive scanning on all electrodes (Inset of Fig. 4 giving the example of ELDH/GCE). This phenomenon could be due to the fact that the oxidative products contaminated the electrode surface, thereby terminating the continuous oxidation of BPA [15,30,31]. So the initial anodic sweep was chosen to investigate the electrochemical behaviors of BPA in this work. At bare GCE (curve a), a smaller oxidation peak could be seen with a higher oxidation potential at 0.525 V, revealing that the direct electrochemistry of BPA was a relatively slow process. While at LDH/GCE (curve b), the oxidation current had been obviously improved at a lower oxidation potential (0.510 V). The enhanced electrochemical performance could be ascribed to the favorable catalytic activity and positively charged surface of LDH. However, ELDH/GCE (curve

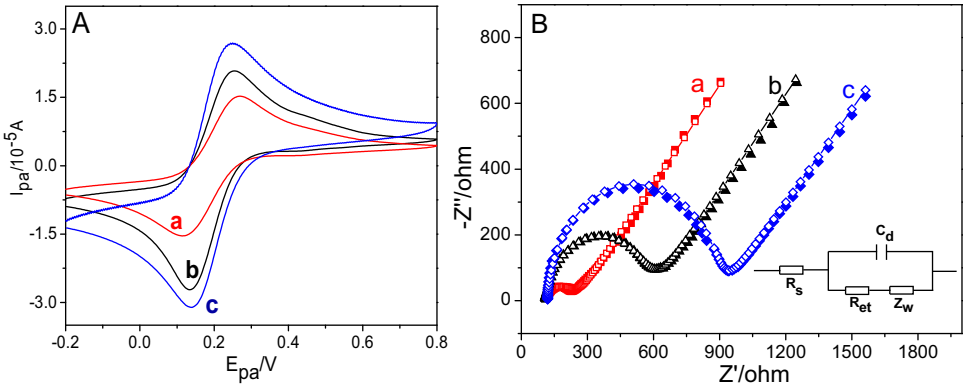

Fig. 3. CVs (A) and Nyquist plots (B) of GCE (a) and LDH/GCE(b) ELDH/GCE(c) in 5 mM $Fe(CN)_6^{3-/4-}$ (1:1) solution containing 0.1 M KCl. (Scan rate: 100 mV/s). In Nyquist plots, measured data were shown as solid symbols with calculated fit to the equivalent circuit as hollow symbols with fitting line. Inset is the Randles circuit.

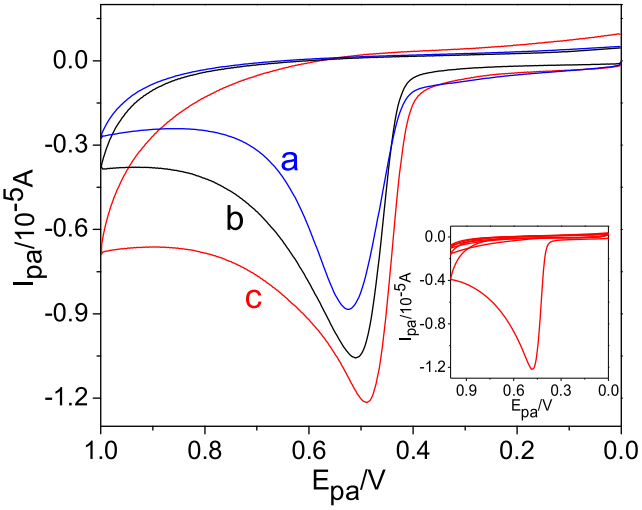

Fig. 4. CVs of GCE(a), LDHs/GCE(b), ELDHs/GCE (c) of 0.1 mM BPA in 0.1 M PBS (pH = 8.5). Scan rate: 100 mV/s. Accumulation time: 100 s. Accumulation potential: −0.3 V. Inset: CV of eldh/GCE with multiple scans in 0.1 mM BPA.

c) exhibits the bigger oxidation peak with more negative anodic potential at 0.489 V than those for LDH/GCE. Its oxidation potential is also smaller than previous reports such as Si/boron-doped electrode (1.2 V, vs. SCE) [14], carbon paste electrode (0.89 V, vs. SCE) [32], GCE (0.65 V, vs. Ag/AgCl) [33] and PAMAM/Fe_3O_4/GCE (0.541 V vs. SCE) [34]. It was supposed that the more exposed active sites and positive charges of ELDH entrapped more BPA molecules for their catalytic oxidation. In other words, exfoliation made the edge-sharing octahedral MO_6 moieties more accessible [21], which could afford more positive charges and coordination-sites for the capture and oxidation of BPA. Moreover, the ultrathin and small size nature with enlarged surface area could also facilitate the electron exchange of BPA with electrode.

3.4. Effects of pH

The effects of pH on the oxidation of BPA at ELDH/GCE were performed in the pH range from 4.5 to 10.5 (Fig. 5A). The oxidation peak currents gradually increase with pH value increasing from 4.5 to 8.5 (Fig. 5B, curve a). When the solution pH exceeds 8.5, the oxidation peak current conversely decreases. The optimal pH value is lower than the pK_a of BPA (pK_a = 9.73) [35], revealing that ELDH could more easily absorb the non-dissociated BPA than the dissociated form in weak alkaline environment. Considering the sensitivity, a pH of 8.5 was chosen for the experiments.

A good linear relationship was observed between the oxidation peak potential (E_{pa}) and pH value (Fig. 5B, curve b), indicating that protons were directly involved in the oxidation of BPA. The linear equation is E_{pa} (V) = −0.053 pH + 0.942 (R = 0.998). The theoretical value for slope can be obtained according to the Nernst equation: dE(mV)/dpH = −59 m/n, where m and n are the number of proton and electron involving electrode reaction. When m is equal to n, the resulting theoretical value of 59 mV pH^{-1} represents the perfectly equal number of proton and electron transfer process [17]. Hence, the slope of 53 mV pH^{-1} for this work can indicate that the number of electron transfer is equivalent to that of proton participating in the electro-oxidation of BPA on ELDH/GCE [17,30].

3.5. Effects of scan rate

CVs of BPA on ELDH/GCE at different scan rate (v) were also determined for further understanding mechanism. As shown in Fig. 6A, the peak currents increase linearly against scan rate in the range from 25 to 350 mV/s, suggesting a typical absorption-controlled process at ELDH/GCE. The result also manifests that ELDH is quite favorable material for the pre-concentration and quantitative analysis of BPA on the modified electrode [36]. Moreover, a linear relationship of E_{pa} vs. ln v was obtained as E_{pa} = 0.372 + 0.026 ln ν (R = 0.998,). As for an adsorption-controlled and totally irreversible electrode process, E_{pa} is defined by the Laviron equation [37]: $E_{pa} = E^0 + (RT/\alpha nF)\ \ln(RTk^0/\alpha nF) + (RT/\alpha nF)\ \ln \nu$, where α is transfer coefficient, k^0 is standard rate constant of the reaction, n is electron transfer number involved in rate-determining step, ν is scan rate, E^0 is formal redox potential, R is the gas constant, T is the absolute temperature, and F is the Faraday constant. Generally, α is assumed to be 0.5 in the totally irreversible electrode process. Thus, according to the slope of above linear correlation, the electron transfer number (n) is calculated to be about 2 (generally taking T = 298 K, R = 8.314 J K^{-1} mol^{-1}, and F = 96480C mol^{-1}). On the whole, the electrooxidation of BPA at ELDH/GCE is a two-electron and two-proton transfer process. Hence, the mechanism for electrocatalytic oxidation of BPA on the fabricated senor could be expressed as follows (Scheme 2).

3.6. Effects of ELDH content, accumulation time and potential

The optimization of ELDH amount on the electrode surface was studied in pH 8.0 PBS solution containing 0.1 mM BPA. In Fig. 7, the oxidation peak current increases with increasing concentration of ELDH from 0 to 8 μL, while decreases with ELDH suspension further increasing. This result might be caused by the aggregated

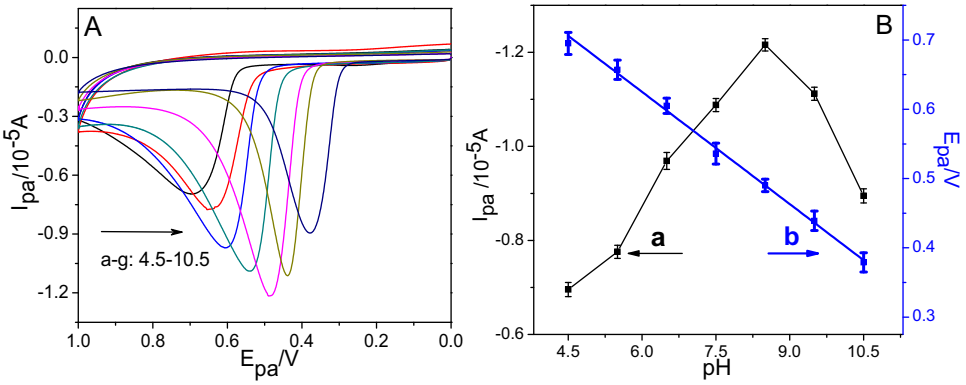

Fig. 5. (A) CVs of 0.1 mM BPA at ELDH/GCE in 0.1 M PBS with different pH values (from a to g: 4.5, 5.5, 6.5, 7.5, 8.5, 9.5 and 10.5). (B) Effects of pH value on the peak current (a) and potential (b) with scan rate at 100 mV/s.

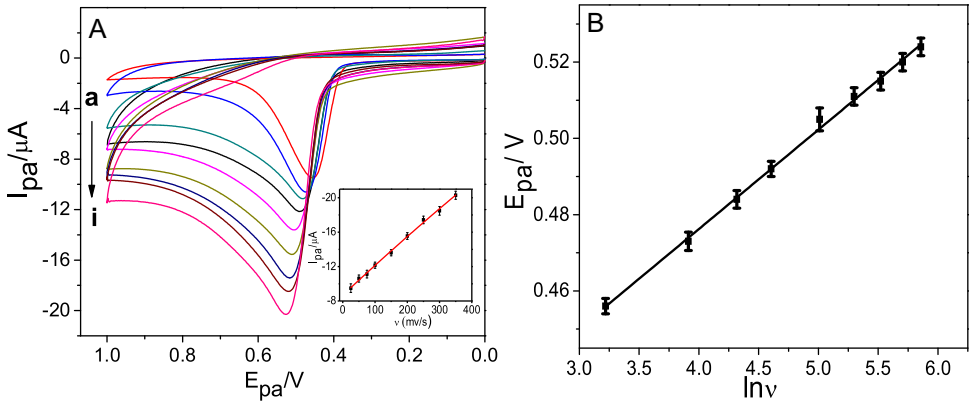

Fig. 6. (A) CVs of 0.1 mM BPA at ELDH/GCE with different scan rates. Curves a-i are obtained at 25, 50, 75, 100, 150, 200, 250 and 300,350 mV/s, respectively. Inset is the plot of the peak current vs. the scan rate. Inset is the plot of the peak current vs. the scan rate. (B) The relationship between E_{pa} and ln v.gr6

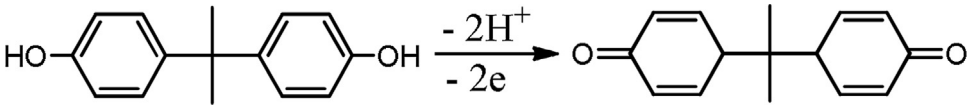

Scheme 2. The possible mechanism for BPA oxidation at ELDH/GCE.

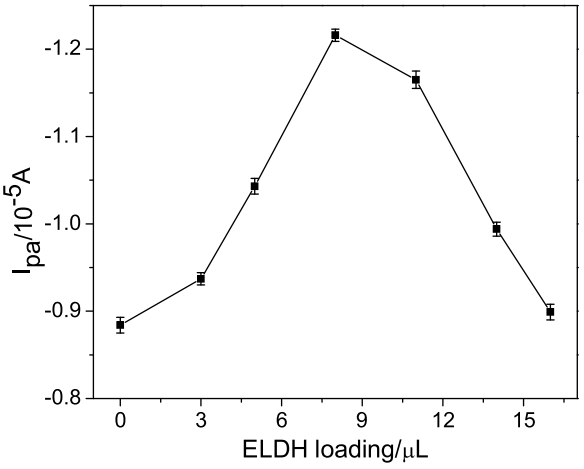

Fig. 7. Dependence of current response for 0.1 mM BPA oxidation in 0.1 M pH 8.5 PBS on ELDH content.

LDH sheets and the increased film thickness, which may lead to the lower electron transfer in BPA oxidation process. Hence, 8 μL of 3 mg mL^{-1} ELDH colloidal solution was used to modify GCE throughout this work.

The adsorption of BPA on the GCE could also affect the current response, so the relationships between the peak current and accumulation time/potential were respectively investigated. As shown in Fig. 8A, the oxidation peak current of BPA gradually increase with accumulation time and reaches saturated and stable after 120 s. It could be speculated that the adsorption and/or exchange of BPA achieved equilibrium at this moment. So the accumulation time was set at 120 s. Fig. 8 B illustrates that the oxidation peak occurs the maximum with the accumulation potential at −0.20 V. Then the peak current decreases with further increasing accumulation potential. Therefore, the accumulation potential of −0.20 V was used in further experiments.

3.7. Chronocoulumetry

The effective surface areas of bare GCE, LDH/GCE and ELDH/GCE can be determined by chronocoulometry in 0.1 mM $K_3[Fe(CN)_6]$

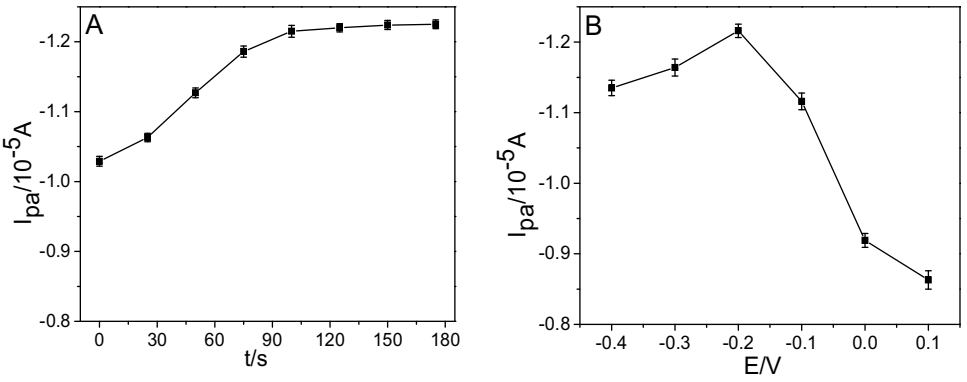

Fig. 8. Effect of accumulation time (A) and accumulation potential (B) on the oxidation peak current of 0.1 mM BPA.

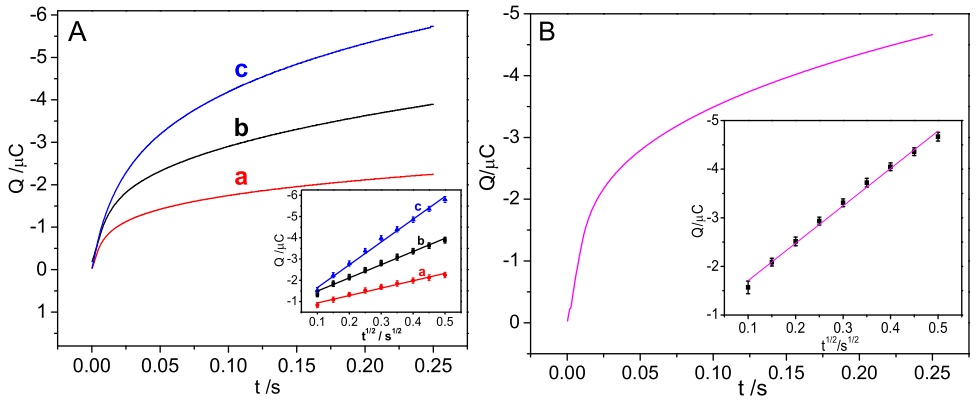

Fig. 9. (A) Plot of *Q*-*t* curves and plots of GCE (a), LDH/GCE (b) and ELDH/GCE (c) in 0.1 mM $K_3[Fe(CN)_6]$ containing 1 M KCl. Inset: plot of *Q*-$t^{1/2}$ curve on GCE (a), LDH/GCE (b) and ELDH/GCE (c). (B) Plot of *Q*–*t* curve of ELDH/GCE in 0.1 M pH 8.5 PBS containing 0.1 mM BPA after background subtracted. Inset: plot of *Q*–$t^{1/2}$ curve on ELDH/GCE.

solution containing 1.0 M KCl. The calculation equation was given by following Anson equation [38].

$$Q(t) = \frac{2nFAcD^{\frac{1}{2}}t^{\frac{1}{2}}}{\pi^{\frac{1}{2}}} + Q_{dl} + Q_{ads} \quad (1)$$

where *A* is the effective surface area of working electrode, *c* is the concentration of substrate, *D* is the standard diffusion coefficient of $[Fe(CN)_6]^{3-}$ (7.6×10^{-6} cm^2 s^{-1} at 25 °C), Q_{dl} is double layer charge which could be eliminated by background subtraction, Q_{ads} is Faradic charge. Basing on the slope of the plot of *Q* vs. $t^{1/2}$ in Fig. 9A, *A* values for GCE, LDH/GCE and ELDH/GCE were calculated to be 0.058 cm^2, 0.104 cm^2 and 0.179 cm^2, respectively. Obviously, ELDH nanosheets modification could increase the electrochemical effective surface area (3 folds of bare GCE), which enhanced the current response toward $K_3[Fe(CN)_6]$ for the proposed sensor. The diffusion coefficient *D* and Faradic charge Q_{ads} of BPA at ELDH/GCE were determined by using chronocoulometry experiments in 0.1 mM BPA PBS (pH 8.5) solution. As illustrated in the inset of Fig. 9B, *Q* is linearly proportional to $t^{1/2}$ with a slope of 7.84×10^{-6} C s$^{1/2}$ and an intercept (Q_{ads}) of 8.78×10^{-7} C. As a result, *D* could be obtained as 4.04×10^{-6} cm^2 s^{-1} according to Equation (1). Based on the equation $Q_{ads} = nFA\Gamma_s$, the adsorption capacity Γ_s of BPA at ELDH/GCE was calculated to be 2.55×10^{-11} mol cm^{-2}. The standard heterogeneous rate constant (k_s) for completely irreversible oxidation of BPA at ELDH/GCE is calculated by the following equation [39]:

$$k_s = 2.415\, exp(-0.02F/RT)D^{1/2}(E_p - E_{p/2})^{-1/2}v^{1/2} \quad (2)$$

where E_p and $E_{p/2}$ stand for the peak potential and the potential at $I = I_p/2$, respectively. In present work, $E_p - E_{p/2} = 34$ mV, $D = 4.04 \times 10^{-6}$ cm^2 s^{-1}, $v = 100$ mV/s and $T = 298$ K. The k_s value was thereby obtained as 3.82×10^{-3} cm s^{-1}, indicating a fast electron transfer process.

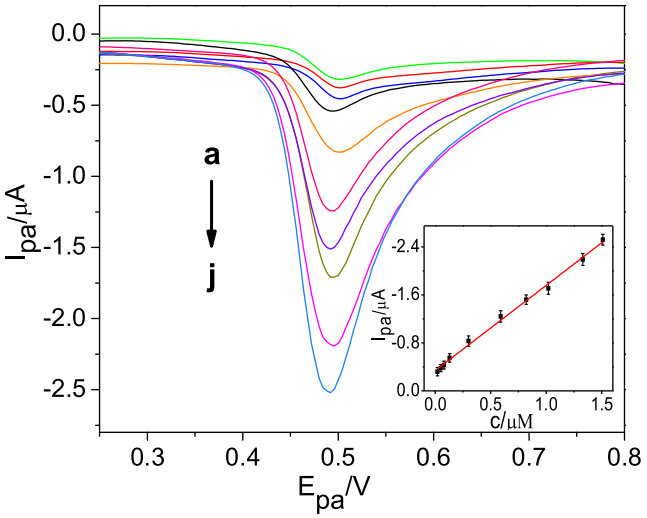

Fig. 10. DPV curves of BPA at ELDH/GCE in 0.1 M pH 8.5 PBS containing different concentrations of BPA (a–j: 0.02–1.5 μM). Insert: liner calibration curve. Amplitude: 0.05 V; pulse width: 0.2 s; pulse period: 0.5 s.

3.8. Differential pulse voltammetric determinations

Differential pulse voltammetrys (DPV) for BPA in various concentrations were performed at ELDH/GCE in the optimum conditions. Fig. 10 displays that the oxidation peak currents are

Table 1
Comparison of proposed sensor for determination of BPA with others.

Modified electrode	Analytical technique	Linear range (μM)	LOD (nM)	Ref.
Tyrs–APTES/nTiO$_2$/Ti	Impedance method	0.01–1	10	[12]
PGA/MWCNT-NH$_2$/GCE	DPV	0.1–10	20	[40]
CoPc-CPE[a]	DPV	0.088–12.5	10	[41]
MCM-41/CPE	DPV	0.22–8.8	38	[17]
GR–IL/GCE	LSV	0.02–2	8	[42]
LDH/GCE	DPV	0.01–1.05	5	[15]
CS/MNPs-rGO/GCE	DPV	0.06–11	16.7	[43]
CS–Fe$_3$O$_4$/GCE	DPV	E 0.05–30	8	[44]
Pt/GR-CNTs/GCE	DPV	0.06–10.0	42	[31]
AuNPs/SGNF/GCE	LSV	0.08–250	35	[45]
CTS-GR/CILE[b]	DPV	0.1–800	26.4	[46]
Boron-doped diamond electrode	DPV	0.44–5.2	210	[47]
ELDH/GCE	DPV	0.02–1.51	6.8	This work

[a] CPE: carbon paste electrode.
[b] CILE: carbon ionic liquid electrode.

Table 2
Interferences of other species on 5 μmol L^{-1} BPA.

Interferents	C (mol L^{-1})	I_{pa} change (%)	Interferents	C (mol L^{-1})	I_{pa} change (%)
Ca^{2+}	5×10^{-4}	−2.7	NO_3^-	5×10^{-4}	−2.3
Mg^{2+}	5×10^{-4}	+3.2	Phenol	2.5×10^{-4}	+5.2
Zn^{2+}	5×10^{-4}	+2.8	Hydroquinone	2.5×10^{-4}	+5.6
Cu^{2+}	5×10^{-4}	−3.1	Hydroxyphenol	2.5×10^{-4}	+4.7
Fe^{3+}	5×10^{-4}	−3.5	Pyrocatechol	2.5×10^{-4}	+4.8
Al^{3+}	5×10^{-4}	−2.9	2-Nitrophenol	2.5×10^{-4}	+5.9
SO_4^{2-}	5×10^{-4}	−2.0	4-Nitrophenol	2.5×10^{-4}	+6.1

proportional to the concentration of BPA in a wider range from 2×10^{-8} to 1.51×10^{-6} M. The linear equation was expressed as I_{pa} *(μA)* = −1.422c(μM) − 0.337 *(R = 0.9977)*, and the detection limit was estimated as 6.8×10^{-9} M (S/N = 3). It can be seen that ELDH/GCE is essentially superior or comparable to the previous reports. The data of comparison are illustrated in Table 1. The lower detection limit can be contributed to the large surface area and more exposed active sites of ELDH nanosheets. Thus, ELDH/GCE could be used as a desirable sensor for BPA detection.

3.9. Reproducibility, stability and selectivity

The reproducibility of ELDH/GCE was investigated by DPV containing 1.5 μM. The relative standard deviation (RSD) for the oxidation peak currents for five determinations is 4.3%, suggesting excellent repeatability of the modified electrode. The modified electrode was also used to detect 1.5 μM BPA after keeping in refrigerator at 4 °C for two weeks. The currents do not show an obvious reduction (lower than 5%), suggesting a good stability. Since the actual samples often containing interfering substances, the influence of possible interferents were studied in 1.5 μM BPA by DPV. The results are listed in Table 2. For 100-fold concentration of Ca^{2+}, Mg^{2+}, Zn^{2+}, Cu^{2+}, Fe^{3+}, Al^{3+}, SO_4^{2-}, NO_3^-, changes of anodic currents are less than 4%, revealing no influence on BPA determination. Moreover, 50-fold concentration of hydroquinone, hydroxyphenol, pyrocatechol, 2-Nitrophenol, 4-Nitrophenol nearly have no influence on the determination of BPA with less than 7% I_{pa} variations. The results demonstrate that the prepared sensor is highly selective toward BPA.

3.10. Real sample analysis

In order to evaluate the performance of the proposed sensor basing on ELDH/GCE, two kinds of milk samples were analyzed. Recovery experiments were carried out by the standard spiked method and the current values are obtained by DPV. The analytic results are outlined in Table 3 and no BPA is found in the milk samples. Additionally, the recovery range is from 95% to 116% with the average RSD of less than 5.1%, indicating that the developed electrochemical sensor can be applied for the detection of BPA in milk samples.

Table 3
Recoveries of BPA from spiked milk samples (n = 5).

Sample	Added (μM)	Found (μM)[a]	Recovery (%)	RSD (%)[b]
Liquid milk	0	0	–	3.1
	0.5	0.56	112	4.1
	1.0	1.16	116	3.5
	1.5	1.46	97	5.1
Milk powder	0	0	–	3.1
	0.5	0.55	110	3.7
	1.0	0.95	95	4.9
	1.5	1.53	102	4.2

[a] Mean of five measurements.
[b] Relative standard deviation for $n = 5$.

4. Conclusion

In this work, the bulk LDH was successfully exfoliated into ultrathin ELDH nanosheets in water medium. Then a sensitive electrochemical sensor of BPA was constructed by modifying GCE with ELDH. It was believed that ELDH nanosheets could accelerate electron transfer through the following aspects. Firstly, ELDH could provide more exposed active sites on the surface of modified materials. Secondly, exfoliation endowed ELDH with larger electrochemical effective surface area. Finally, the better dispersity of ELDH could afford a lower mass transfer resistance. As a consequence, the proposed ELDH/GCE showed excellent electrocatalytic capability toward the oxidation of BPA. The more number of active sites and large effective surface area had remarkably enhanced the oxidation peak response and decreased the oxidation overpotential. The fabricated sensor displayed a low detection limit with satisfactory reproducibility, stability and selectivity. Therefore, the prepared sensor had been successfully applied for the determina-

tion of milk samples. Additionally, this new sensor was prepared in a simple procedure with low cost.

Acknowledgements

This study was supported by the National Natural Science Foundation of China (21173135, 21403121, 21573133, 21275085), the Natural Science Foundation of Shandong Province, China (ZR2014JL013 and ZR2013BQ013), the open foundation from the Key Laboratory of Marine Bioactive Substance and Modern Analysis Technology, SOA (MBSMAT-2015-04, MBSMAT-2014-02, MBSMAT-2013-01 and MBSMAT-2012-07.).

References

[1] E. Burridge, A. Bisphenol, Product profile, Eur. Chem. News 17 (2003) 14–20.
[2] K.V. Ragavan, N.K. Rastogi, M.S. Thakur, Sensors and biosensors for analysis of bisphenol-A, TrAC Trends Anal. Chem. 52 (2013) 248–260.
[3] P. Fu, K. Kawamura, Ubiquity of bisphenol A in the atmosphere, Environ. Pollut. 158 (2010) 3138–3143.
[4] D.C. Apodaca, R.B. Pernites, R. Ponnapati, F.R.D. Mundo, R.C. Advincula, Electropolymerized molecularly imprinted polymer film: EIS sensing of bisphenol a, Macromolecules 44 (2011) 6669–6682.
[5] K.K. Reza, M.A. Ali, S. Srivastava, V.V. Agrawal, A.M. Biradar, Tyrosinase conjugated reduced graphene oxide based biointerface for bisphenol A sensor, Biosens. Bioelectron. 74 (2015) 644–650.
[6] X. Xin, S. Sun, H. Li, M. Wang, R. Jia, Electrochemical bisphenol A sensor based on core-shell multiwalled carbon nanotubes/graphene oxide nanoribbons, Sens. Actuators B 209 (2015) 275–280.
[7] M.P. Zhao, Y.Z. Li, Z.Q. Guo, X.X. Zhang, W.B. Chang, A new competitive enzyme-linked immunosorbent assay (ELISA) for determination of estrogenic bisphenols, Talanta 57 (2002) 1205–1210.
[8] C. Hou, W. Tang, C. Zhang, Y. Wang, N. Zhu, A novel and sensitive electrochemical sensor for bisphenol A determination based on carbon black supporting ferroferric oxide nanoparticles, Electrochim. Acta 144 (2014) 324–331.
[9] K.V. Ragavan, N.K. Rastogi, Graphene-copper oxide nanocomposite with intrinsic peroxidase activity for enhancement of chemiluminescence signals and its application for detection of Bisphenol-A, Sens. Actuators B 229 (2016) 570–580.
[10] F. Cheng, N.M. Bandaru, A.V. Ellis, N.H. Voelcker, Beta-cyclodextrin decorated nanostructured SERS substrates facilitate selective detection of endocrine disruptor chemicals, Biosens. Bioelectron. 42 (2013) 632–639.
[11] K.V. Ragavan, L.S. Selvakumar, M.S. Thakur, Functionalized aptamers as nano-bioprobes for ultrasensitive detection of bisphenol-A, Chem. Commun. 49 (2013) 5960–5962.
[12] N. Singh, K.K. Reza, M.A. Ali, V.V. Agrawal, A.M. Biradar, Self assembled DC sputtered nanostructured rutile TiO2 platform for bisphenol A detection, Biosens. Bioelectron. 68 (2015) 633–641.
[13] K.K. Reza, N. Singh, S.K. Yadav, M.K. Singh, A.M. Biradar, Pearl shaped highly sensitive Mn3O4 nanocomposite interface for biosensor applications, Biosens. Bioelectron. 62 (2014) 47–51.
[14] M. Murugananthan, S. Yoshihara, T. Rakuma, T. Shirakashi, Mineralization of bisphenol A (BPA) by anodic oxidation with boron-doped diamond (BDD) electrode, J. Hazard. Mater. 154 (2008) 213–220.
[15] H. Yin, L. Cui, S. Ai, H. Fan, L. Zhu, Electrochemical determination of bisphenol A at Mg-Al-CO3 layered double hydroxide modified glassy carbon electrode, Electrochim. Acta 55 (2010) 603–610.
[16] Y. Long, Z. Hui, S. Fan, S. Deng, L. Qi, L. Jie, C.P. Li, Label-free electrochemical immunosensor based on gold-silicon carbide nanocomposites for sensitive detection of human chorionic gonadotrophin, Biosens. Bioelectron. 57C (2014) 199–206.
[17] F. Wang, J. Yang, K. Wu, Mesoporous silica-based electrochemical sensor for sensitive determination of environmental hormone bisphenol A, Anal. Chim. Acta 638 (2009) 23–28.
[18] H. Yin, Y. Zhou, S. Ai, Q. Chen, X. Zhu, X. Liu, L. Zhu, Sensitivity and selectivity determination of BPA in real water samples using PAMAM dendrimer and CoTe quantum dots modified glassy carbon electrode, J. Hazard. Mater. 174 (2010) 236–243.
[19] Z. Ye, C. Zhou, X. Yan, Y. Yan, W. Qiang, Aptamer-functionalized nanoporous gold film for high-performance direct electrochemical detection of bisphenol A in human serum, Anal. Chim. Acta 883 (2015) 81–89.
[20] J.H. Choy, S.Y. Kwak, J.S. Park, Y.J. Jeong, J. Portier, Intercalative nanohybrids of nucleoside monophosphates and DNA in layered metal hydroxide, J. Am. Chem. Soc. 121 (1999).
[21] F. Song, X. Hu, Exfoliation of layered double hydroxides for enhanced oxygen evolution catalysis, Nat. Commun. 5 (2014), 4477–4477.
[22] S. Cho, J.W. Jang, Y.B. Park, J.Y. Kim, G. Magesh, H.K. Jin, M. Seol, K. Yong, K.H. Lee, J.S. Lee, An exceptionally facile method to produce layered double hydroxides on a conducting substrate and their application for solar water splitting without an external bias, Energy Environ. Sci. 7 (2014) 2301–2307.
[23] G. Fan, F. Li, D.G. Evans, X. Duan, ChemInform abstract: catalytic applications of layered double hydroxides: recent advances and perspectives, Chem. Soc. Rev 43 (2014) 7040–7066.
[24] D. Shan, S. Cosnier, C. Mousty, Layered double hydroxides: an attractive material for electrochemical biosensor design, Anal. Chem. 75 (2003), págs. 3872–3879.
[25] E. Han, S. Dan, H. Xue, Hybrid material based on chitosan and layered double hydroxides: characterization and application to the design of amperometric phenol biosensor, Biomacromolecules 8 (2007) 971–975.
[26] T. Zhan, X. Wang, X. Li, Y. Song, W. Hou, Hemoglobin immobilized in exfoliated Co_2Al LDH-graphene nanocomposite film: direct electrochemistry and electrocatalysis toward trichloroacetic acid, Sens. Actuators B 228 (2016) 101–108.
[27] L. Chen, B. Sun, X. Wang, F. Qiao, S. Ai, 2D ultrathin nanosheets of Co-Al layered double hydroxides prepared in L-asparagine solution: enhanced peroxidase-like activity and colorimetric detection of glucose, J. Mater. Chem. B 1 (2013) 2268–2274.
[28] Z. Ling, J. Wang, D. Li, Y. Li, An electrochemical aptasensor based on gold nanoparticles dotted graphene modified glassy carbon electrode for label-free detection of bisphenol A in milk samples, Food Chem. 162 (2014) 34–40.
[29] Z. Liu, R. Ma, M. Osada, N. Iyi, Y. Ebina, K. Takada, T. Sasaki, Synthesis, anion exchange, and delamination of Co-Al layered double hydroxide: assembly of the exfoliated nanosheet/polyanion composite films and magneto-optical studies, J. Am. Chem. Soc. 128 (2006) 4872–4880.
[30] T. Zhan, Y. Song, X. Li, W. Hou, Electrochemical sensor for bisphenol A based on ionic liquid functionalized Zn-Al layered double hydroxide modified electrode, Mater. Sci. Eng. C 64 (2016) 354–361.
[31] Z. Zheng, Y. Du, Z. Wang, Q. Feng, C. Wang, Pt/graphene-CNTs nanocomposite based electrochemical sensors for the determination of endocrine disruptor bisphenol A in thermal printing papers, Analyst 138 (2013) 693–701.
[32] W. Huang, Voltammetric determination of bisphenol a using a carbon paste electrode based on the enhancement effect of cetyltrimethylammonium bromide (CTAB), Bull. Korean Chem. Soc. 26 (2005) 1560–1564.
[33] H. Kuramitz, M. Matsushita, S. Tanaka, Electrochemical removal of bisphenol A based on the anodic polymerization using a column type carbon fiber electrode, Water Res. 38 (2004) 2331–2338.
[34] H. Yin, L. Cui, Q. Chen, W. Shi, S. Ai, L. Zhu, L. Lu, Amperometric determination of bisphenol A in milk using PAMAM-Fe3O4 modified glassy carbon electrode, Food Chem. 125 (2011) 1097–1103.
[35] Y. Zhang, L. Wang, D. Lu, X. Shi, C. Wang, X. Duan, Sensitive determination of bisphenol A base on arginine functionalized nanocomposite graphene film, Electrochim. Acta 80 (2012) 77–83.
[36] A.J. Bard, H.D. Abruna, C.E. Chidsey, L.R. Faulkner, S.W. Feldberg, K. Itaya, M. Majda, O. Melroy, R.W. Murray, M.D. Porter, ChemInform abstract: the electrode/electrolyte interface-A status report, Cheminform 24 (2010) 7147–7173.
[37] E. Laviron, Adsorption, autoinhibition and autocatalysis in polarography and in linear potential sweep voltammetry, J. Electroanal. Chem. 52 (1974) 355–393.
[38] F.C. Anson, Application of potentiostatic current integration to the study of the adsorption of cobalt(III)-(ethylenedinitrilo(tetraacetate) on mercury electrodes, Anal. Chem. 75 (1969) 313–315.
[39] N. Ralph, Electrochemistry at Solid Electrodes, 1969.
[40] Y. Lin, K. Liu, C. Liu, Y. Lu, K. Qian, L. Li, L. Bo, Electrochemical sensing of bisphenol A based on polyglutamic acid/amino-functionalised carbon nanotubes nanocomposite, Electrochim. Acta 133 (2014) 492–500.
[41] H.S. Yin, Y.L. Zhou, S.Y. Ai, Preparation and characteristic of cobalt phthalocyanine modified carbon paste electrode for bisphenol A detection, J. Electroanal. Chem. 626 (2009) 80–88.
[42] J. Ping, X. Zhang, Z. Wu, B. Lei, Y. Xu, C. Liang, W. Cao, Electrochemical sensing of bisphenol A by graphene-1-butyl-3-methylimidazolium hexafluorophosphate modified electrode, Talanta 141 (2015) 41–46.
[43] Y. Zhang, Y. Cheng, Y. Zhou, B. Li, G. Wei, X. Shi, Y. Xian, Electrochemical sensor for bisphenol A based on magnetic nanoparticles decorated reduced graphene oxide, Talanta 107 (2013) 211–218.
[44] C. Yu, L. Gou, X. Zhou, N. Bao, H. Gu, Chitosan-Fe_3O_4 nanocomposite based electrochemical sensors for the determination of bisphenol A, Electrochim. Acta 56 (2011) 9056–9063.
[45] X. Niu, Y. Wu, G. Wang, R. Jie, G. Hao, J. Gao, A novel electrochemical sensor of bisphenol A based on stacked graphene nanofibers/gold nanoparticles composite modified glassy carbon electrode, Electrochim. Acta 98 (2013) 167–175.
[46] Q. Wang, Y. Wang, S. Liu, L. Wang, G. Feng, G. Fei, S. Wei, Voltammetric detection of bisphenol a by a chitosan-graphene composite modified carbon ionic liquid electrode, Thin Solid Films 520 (2012) 4459–4464.
[47] M. Portaccio, D.D. Tuoro, F. Arduini, D. Moscone, M. Cammarota, D.G. Mita, M. Lepore, Laccase biosensor based on screen-printed electrode modified with thionine-carbon black nanocomposite, for Bisphenol A detection, Electrochim. Acta 109 (2013) 340–347.

Biographies

Tianrong Zhan is an associated professor in College of Chemistry and Molecular Engineering, Qingdao University of Science and Technology. He received his

Ph.D. degree from Institute of Oceanology, Chinese Academy of Science in 2004. He worked in the School of Pharmaceutical sciences and the School of chemistry and chemical engineering of Shandong University as a postdoctoral research fellow from 2004 to 2006, and 2009 to 2011, respectively. Now his research concentrates on colloid and interface sciences and electrochemical sensor.

Yang Song is a master candidate in Qingdao University of Science and Technology. She majors in preparation of layered double hydroxides composite.

Zhengwei Tan is a master candidate in Qingdao University of Science and Technology. He majors in layered double hydroxides modified electrode.

Wanguo Hou received his MS and PhD degree from the Chemistry Department of Shandong University in 1986 and 1989, respectively. He is presently a professor in the School of chemistry and chemical engineering, Shandong University. His main research interests are in colloid and interface chemistry, micro(nano)materials, dispersion system, and oilfield chemistry.